

Domain Generalization for Cross-Receiver Radio Frequency Fingerprint Identification

Ying Zhang, Qiang Li[†], Hongli Liu, Liu Yang and Jian Yang

Abstract—Radio Frequency Fingerprint Identification (RFFI) technology uniquely identifies emitters by analyzing unique distortions in the transmitted signal caused by non-ideal hardware. Recently, RFFI based on deep learning methods has gained popularity and is seen as a promising way to address the device authentication problem for Internet of Things (IoT) systems. However, in *cross-receiver* scenarios, where the RFFI model is trained over RF signals from some receivers but deployed at a new receiver, the alteration of receiver’s characteristics would lead to data distribution shift and cause significant performance degradation at the new receiver. To address this problem, we first perform a theoretical analysis of the cross-receiver generalization error bound and propose a sufficient condition, named Separable Condition (SC), to minimize the classification error probability on the new receiver. Guided by the SC, a Receiver-Independent Emitter Identification (RIEI) model is devised to decouple the received signals into emitter-related features and receiver-related features and only the emitter-related features are used for identification. Furthermore, by leveraging federated learning, we also develop a FedRIEI model to eliminate the need for centralized collection of raw data from multiple receivers. Experiments on two real-world datasets demonstrate the superiority of our proposed methods over some baseline methods.

Index Terms—Radio Frequency Fingerprint Identification, domain generalization, feature disentanglement, Federated Learning.

I. INTRODUCTION

WITH the rapid development of wireless communication technology, the utilization of Internet of Things (IoT) devices and technologies has increased significantly in critical applications such as smart healthcare, smart cities, and intelligent vehicles. However, due to the open nature of wireless channels, their security is more susceptible to illegal eavesdropping and malicious attacks compared to traditional wired networks [2]. Therefore, in meeting the growing demand for wireless communication, the pursuit of more efficient and simpler wireless communication security authentication and protection technologies becomes increasingly crucial. Most of the traditional wireless communication networks use cryptographic mechanisms and security protocols to ensure network security, which may not be feasible for wireless IoT devices due to their limited energy and computational resources [3], [4].

This work was supported in part by the National Natural Science Foundation of China under Grant 62171110.

Y. Zhang, Q. Li, H. Liu and L. Yang are with School of Information and Communication Engineering, University of Electronic Science and Technology of China, Chengdu, P. R. China, 611731. J. Yang is with Beijing Institute of Technology, Beijing, P. R. China, 100081, and also with Laboratory of Electromagnetic Space Cognition and Intelligent Control, Beijing, P. R. China, 100083. Part of this work has been published in IEEE SPAWC 2023 [1].

[†] Corresponding author. E-mail: lq@uestc.edu.cn

Radio Frequency Fingerprint Identification (RFFI) is an effective identification and authentication technique for wireless communication devices at the physical layer, widely employed in various IoT applications [5]–[7]. It distinguishes different devices based on unique radio frequency (RF) fingerprint features within the signals of wireless transmitting devices [8]. These fingerprint features primarily arise from the non-ideal characteristics of the devices, e.g. D/A, filter, mixer and amplifier, which introduce subtle unintentional modulation in the transmit signal. This unintentional modulation gives rise to unique fingerprint for each emitter, which is difficult to be imitated and tampered by illegal users. Therefore, the RFFI technique can serve as a means of identifying legitimate users and securing wireless communication networks at the physical layer.

The earlier RFFI techniques primarily depend on statistical analysis of features extracted from RF signals, such as signal strength, bandwidth, and phase noise [9]–[11]. They mainly focused on using manually crafted features for classification, relying heavily on domain knowledge and experts for feature extraction [12]. Furthermore, the significance of these features is non-deterministic and task-dependent. In recent years, deep learning (DL) approaches have emerged as a promising tool for RFFI. Compared to traditional methods, DL approaches can capture fine-grained features in RF signals, leading to more accurate and robust identification [13]–[16]. Deep learning models do not require manual feature engineering, allowing them to learn complex representations of RF signals automatically, making them well-suited for handling complex wireless signals.

In practice, a model may be trained and deployed with data collected from different receivers. However, the impact of the receiver is often overlooked in current RFFI studies. Similar to the emission stage, the non-ideal characteristics of receiver circuits, such as low-noise amplifiers (LNA), analog-to-digital conversions (ADC), matched filters, etc., inevitably introduce signal distortion. This phenomenon is known as receiver fingerprint contamination. Consequently, the data distributions exhibit significant variations across different receivers. On the other hand, existing DL-based RFFI models usually require identical distributions for both training and testing stages. As such, the alteration of receiver results in decline in recognition performance, especially when the trained model needs to generalize to a new receiver [1], [17].

To mitigate the influence of receivers, recent studies [18]–[20] have employed both labeled training data and unlabeled test data for joint model training. These methods are categorized as Domain Adaptation (DA), which entails transferring

model knowledge from the source domain (i.e. the training receivers) to a target domain (i.e. the new receiver) with accessible target domain data. However, practical challenges often restrict access to target domain data due to privacy issues, regulatory constraints, or the high costs of data acquisition. Consequently, a more viable approach involves training the model using data from multiple receivers, aiming to develop a cross-receiver RFFI model that can be deployed universally once training is complete. This problem, known as cross-receiver RFFI [21], [22], has received scant attention in the current literature.

Cross-receiver RFFI shares similarities with domain generalization (DG) [23]. Inspired by DG, we have developed a cross-receiver RFFI approach, known as the Receiver-Independent Emitter Identification (RIEI) network. The key idea of RIEI is to disentangle the extracted features into the receiver-dependent feature and the emitter-dependent feature via introducing the cross entropy loss, the mutual independence loss and the information entropy loss. These features are then processed such that only the emitter-related features are passed to the subsequent classification network. As a result, we attain a robust RFFI model that is insensitive to the receiver characteristics and has good generalization ability to new receivers.

The RIEI model is trained using centralized data collection and processing, where all RF signals are collected, stored, and processed on a central server. However, practical scenarios involve data originating from various platforms and terminals, which are often stored in a distributed manner. Moreover, uploading data to a central server for centralized learning poses risks of privacy breaches and challenges associated with transmitting large volumes of raw RF data. To address these challenges, we also develop a distributed RIEI model by leveraging federated learning [24]. In experiments, we evaluated RIEI against baseline methods that do not account for cross-receiver effects in a centralized setting. Here, when the inputs are time-domain signals, our proposed method improves accuracy by 10.84% and 9.37% on the HackRF and Wisig real-world datasets, respectively (resp.). When the inputs are time-frequency diagrams, our proposed method improves accuracy by 20.74% and 9.49% on the HackRF and Wisig datasets, resp. In distributed scenarios, compared to baseline methods that disregard receiver impacts, our approach showed 11.24% increase in accuracy, even surpassing the centralized training.

Our contributions are summarized as follows:

- We consider cross-receiver RFFI, and aim at developing a receiver-independent RFFI model, which can effectively address the performance degradation caused by the receivers. And we provide a theoretical analysis of the cross-receiver generalization error bound and propose a sufficient condition, named Separable Condition (SC), to minimize the classification error probability on the new receiver.
- Guided by SC, we devise a novel RIEI model for achieving cross-receiver RFFI. The RIEI exploits training data from multiple receivers to learn a receiver-independent feature space, thereby eliminating the effect of receivers.

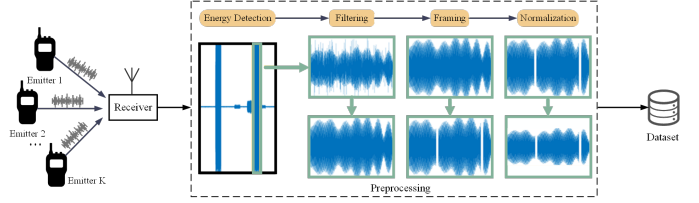


Fig. 1: The signal preprocessing flow.

- We also developed a distributed RIEI model, which obviates the need for central collection of raw data from multiple devices, thereby addressing challenges related to distributed data storage, data transmission, and data privacy.

The remainder of the paper is organized as follows. Sec. II introduces the cross-receiver RFFI problem. Sec. III first conducts a theoretical analysis of cross-receiver RFFI, and then describes the proposed RIEI scheme and its training process. Sec. IV extends RIEI to distributed scenarios. Sec. V presents the experimental results. Sec. VI concludes the paper.

II. PROBLEM FORMULATION

Let us start with the received signal model of RFFI. During the ℓ -th time interval, the received signal can be expressed as

$$x_\ell(t) = \psi(c(t) * \varphi(s(t) \cos(\omega_0 t + \theta))) + n(t), \quad (1)$$

where $(\ell - 1)T \leq t \leq \ell T$, $n(t)$ is the noise, T is the length of the interval, ω_0 is the angular frequency, θ is the initial phase angle, $s(t)$ is random modulating signal, $c(t)$ denotes the channel response, the operator $*$ denotes convolution, $\varphi(\cdot)$ is a random function modeling nonlinear distortion induced by the emitter's hardware, which encodes the "fingerprint" of the emitter, and $\psi(\cdot)$ is a random function modeling the nonlinear reception characteristics induced by the receiver's hardware. Notice that different emitters and receivers have distinct φ and ψ , resp.

As shown in Fig. 1, we usually perform signal preprocessing on the received signal. The preprocessing mainly includes energy detection, filtering, framing and normalization. After signal preprocessing, we have a collection of labeled random RF data $\mathcal{S} = \{\mathcal{S}^1, \dots, \mathcal{S}^K\}$ from K receivers, and $\mathcal{S}^k = \{(x_{k_i}, y_{k_i})\}_{i=1}^{N_k}$ records N_k RF waveform samples x_{k_i} and its emitter index/label $y_{k_i} \in \mathcal{Y} = \{1, \dots, M\}$, where \mathcal{Y} denotes the set of emitters. Due to receiver fingerprint contamination, the joint distribution P_{XY} varies across the receivers, i.e. $P_{XY}^m \neq P_{XY}^n, 1 \leq m \neq n \leq K$. Our goal is to learn a robust and generalizable classification model $h : \mathcal{X} \rightarrow \mathcal{Y}$ that maps the input space to the emitters' index set to achieve a minimum classification error on unseen test data $\mathcal{S}^T = \{x_{\mathcal{T}_i}\}_{i=1}^{N_{\mathcal{T}}}$ obtained from a new receiver with $P_{XY}^T \neq P_{XY}^m$ for $m \in \{1, \dots, K\}$.

Now, the multi-source cross-receiver RFFI problem can be described as follows (cf. Fig. 2). We are interested in training a classification model h^* across the clients, which also minimizes the classification error probability on the unseen test domains \mathcal{S}^T , viz.,

$$h^* = \arg \min_{h \in \mathcal{H}} \epsilon^T(h) \triangleq \mathbb{E}_{(X, Y) \sim P_{XY}^T} [\mathbb{I}(h(X) \neq Y)] \quad (2)$$

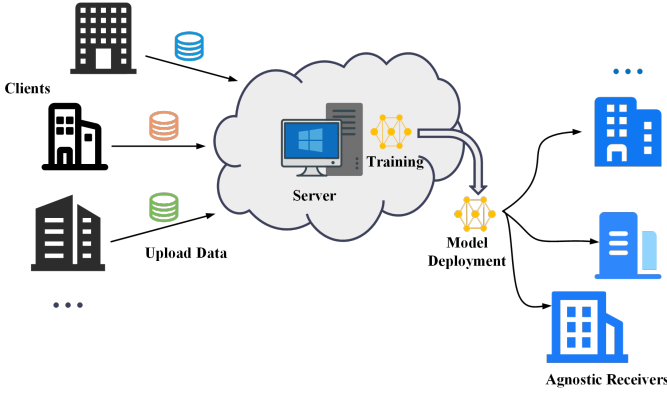


Fig. 2: The scenario of cross-receiver RFFI. First, the server collects raw data from multiple receivers. Then, the server utilizes multi-receiver data to train an RFFI model. Finally, the trained model is deployed directly to new, unseen receivers.

where $\epsilon^T(h)$ denote expected error probability on the test domain, \mathcal{H} denotes a presumed hypothesis space consisting of the classification models, \mathbb{E} denotes the expectation, $\mathbb{I}(\cdot)$ is the indicator function and $\mathbb{I}(a \neq b) = 1$ if $a \neq b$, and 0 otherwise.

Problem (2) is challenging due to the inaccessibility of the joint distribution P_{XY}^T or its realization \mathcal{S}^T . In the following, we will provide an alternative way to indirectly minimize the classification error probability over P_{XY}^T .

III. PROPOSED METHOD

A. Theoretical Analysis

We first make a theoretical analysis of the cross-receiver RFFI problem, which will also shed light on the subsequent method development.

The following lemma characterizes the generalization performance in the target domain.

Lemma 1: Let \mathcal{H} be a hypothesis space of VC dimension d . If \mathcal{S}, \mathcal{T} contains samples of size N each, then for any $\rho \in (0, 1)$, with probability at least $1 - \rho$ (over the choice of the samples), for every $h \in \mathcal{H}$ the following inequality holds

$$\epsilon^t(h) \leq \epsilon^s(h) + \frac{1}{2} d_{\mathcal{H}\Delta\mathcal{H}}(\mathcal{D}^s, \mathcal{D}^t) + \Lambda, \quad (3)$$

where $\epsilon^t(h)$ and $\epsilon^s(h)$ denote expected error probability on the source and target domain, resp., $\Lambda = 4\sqrt{\frac{2d \log 2N + \log \frac{2}{\rho}}{N}} + \Lambda^*$, $\Lambda^* = \min_{h \in \mathcal{H}} \epsilon^s(h) + \epsilon^t(h)$ denotes the minimum combined error probability on both domains, $d_{\mathcal{H}\Delta\mathcal{H}}(\mathcal{D}^s, \mathcal{D}^t) = 2 \sup_{h, h' \in \mathcal{H}} |\mathbb{E}_{X \sim \mathcal{D}^s} [h(X) - h'(X)] - \mathbb{E}_{X \sim \mathcal{D}^t} [h(X) - h'(X)]|$ represents the discrepancy of \mathcal{S} and \mathcal{T} with respect to \mathcal{H} , \mathcal{D}^s and \mathcal{D}^t represent the source and target domain, resp.

From Lemma 1, we see that to minimize the classification error probability on the unseen target domain, we should make the source domain risk $\epsilon^s(h)$ and the domain discrepancy $d_{\mathcal{H}\Delta\mathcal{H}}(\mathcal{D}^s, \mathcal{D}^t)$ as small as possible. For the former, it can be attained by standard supervised learning with labeled source training data. However, for the latter, if we do not impose any constraint on the target domain, the domain discrepancy

could be arbitrarily large. In light of this, we make the following model assumption on data generalization to facilitate the analysis.

Assumption 1 (Domain transformation model [25]): Let X denote the emitter-related variable and ν denote receiver/domain-related variable. We assume that there exists a measurable function $G: \mathcal{X} \times \nu \rightarrow \mathcal{X}$, referred to as a domain transformation model, which parameterizes the inter-domain covariate shift via

$$\mathbb{P}(X^\nu) =^d G\#(\mathbb{P}(X) \times \mathbb{P}(\nu)), \quad (4)$$

where $\#$ denotes the push-forward measure and $=^d$ denotes equality in distribution.

In addition, we introduce the following definition.

Definition 1 (Separable Condition): Let $\tilde{\mathcal{D}}$ be feature space associated with \mathcal{D} and \tilde{h} be an equivalent learning model of $h \in \mathcal{H}$ in the feature space, i.e. $h(X^\nu) = \tilde{h}(Z)$ for some $Z \in \tilde{\mathcal{D}}$. Then, X^ν is called separable under \mathcal{H} if for any $X^\nu \in \mathcal{D}$ and $h \in \mathcal{H}$, the $Z \in \tilde{\mathcal{D}}$ admits a decomposition $Z = [Z_X, Z_\nu]$, which satisfies

- 1) $\nu \rightarrow X \rightarrow Z_X$, i.e. given X , Z_X is independent of ν .
- 2) $X \rightarrow \nu \rightarrow Z_\nu$, i.e. given ν , Z_ν is independent of X .
- 3) $Z_X \perp Z_\nu$, i.e., Z_X is statistically independent of Z_ν .

The following result characterizes $d_{\mathcal{H}\Delta\mathcal{H}}(\mathcal{D}^s, \mathcal{D}^t)$ under the transformation model.

Proposition 1: Suppose that Assumption 1 holds and X^ν satisfies the separable condition on both \mathcal{D}^s and \mathcal{D}^t . Then,

$$d_{\mathcal{H}\Delta\mathcal{H}}(\mathcal{D}^s, \mathcal{D}^t) = 0 \quad (5)$$

if $h(X^\nu) = \tilde{h}(Z_X)$, $\forall X^\nu \in \{\mathcal{D}^s, \mathcal{D}^t\}$.

Before presenting the proof of Proposition 1, we remark that the condition $h(X^\nu) = \tilde{h}(Z_X)$ can be easily fulfilled by just discarding the emitter-irrelevant feature Z_ν and making prediction only based on Z_X .

Proof.

$$\begin{aligned} & d_{\mathcal{H}\Delta\mathcal{H}}(\mathcal{D}^s, \mathcal{D}^t) \\ &= 2 \sup_{h, h' \in \mathcal{H}} \left| \mathbb{E}_{X^{\nu_s} \sim \mathcal{D}^s} [h(X^{\nu_s}) - h'(X^{\nu_s})] \right. \\ & \quad \left. - \mathbb{E}_{X^{\nu_t} \sim \mathcal{D}^t} [h(X^{\nu_t}) - h'(X^{\nu_t})] \right| \\ &= 2 \sup_{h, h' \in \mathcal{H}} \left| \mathbb{E}_{Z \sim \tilde{\mathcal{D}}^s} [h(X^{\nu_s}) \right. \\ & \quad \left. - h'(X^{\nu_s})] - \mathbb{E}_{Z \sim \tilde{\mathcal{D}}^t} [h(X^{\nu_t}) - h'(X^{\nu_t})] \right| \\ &= 2 \sup_{h, h' \in \mathcal{H}} \left| \mathbb{E}_{Z_X, Z_{\nu_s} \sim \tilde{\mathcal{D}}^s} [h(X^{\nu_s}) - h'(X^{\nu_s})] \right. \\ & \quad \left. - \mathbb{E}_{Z_X, Z_{\nu_t} \sim \tilde{\mathcal{D}}^t} [h(X^{\nu_t}) - h'(X^{\nu_t})] \right|. \end{aligned} \quad (6)$$

Notice that

$$\begin{aligned} & \mathbb{E}_{Z_X, Z_{\nu_s} \sim \tilde{\mathcal{D}}^s} [h(X^{\nu_s}) - h'(X^{\nu_s})] \\ &= \mathbb{E}_{X, \nu_s} \mathbb{E}_{Z_X, Z_{\nu_s} | X, \nu_s} [h(X^{\nu_s}) - h'(X^{\nu_s})] \\ &= \mathbb{E}_{\nu_s} \mathbb{E}_X \mathbb{E}_{Z_X, Z_{\nu_s} | X, \nu_s} [h(X^{\nu_s}) - h'(X^{\nu_s})] \\ &= \mathbb{E}_{\nu_s} \mathbb{E}_X \mathbb{E}_{Z_{\nu_s} | \nu_s} \mathbb{E}_{Z_X | X} [h(X^{\nu_s}) - h'(X^{\nu_s})] \\ &= \mathbb{E}_{Z_{\nu_s}, \nu_s} \mathbb{E}_{Z_X, X} [h(X^{\nu_s}) - h'(X^{\nu_s})], \end{aligned} \quad (7)$$

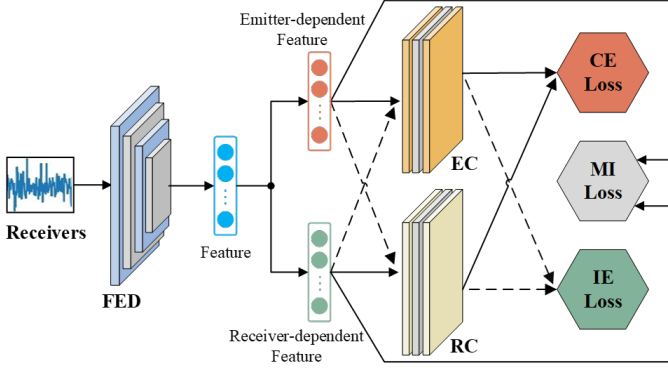


Fig. 3: Illustration of the proposed RIEI method.

where the third equality is due to separable condition. Moreover, if $h(X^\nu) = \tilde{h}(Z_X)$, $\forall X^\nu \in \{\mathcal{D}^s, \mathcal{D}^t\}$, then (7) can be further expressed as

$$\begin{aligned} & \mathbb{E}_{Z_X, Z_{\nu_s} \sim \tilde{\mathcal{D}}^s} |h(X^{\nu_s}) - h'(X^{\nu_s})| \\ &= \mathbb{E}_{Z_{\nu_s}, \nu_s} \mathbb{E}_{Z_X, X} |\tilde{h}(Z_X) - \tilde{h}'(Z_X)| \\ &= \mathbb{E}_{Z_X, X} |\tilde{h}(Z_X) - \tilde{h}'(Z_X)|. \end{aligned} \quad (8)$$

Similarly, we have

$$\begin{aligned} & \mathbb{E}_{Z_X, Z_{\nu_t} \sim \tilde{\mathcal{D}}^t} |h(X^{\nu_t}) - h'(X^{\nu_t})| \\ &= \mathbb{E}_{Z_X, X} |\tilde{h}(Z_X) - \tilde{h}'(Z_X)|. \end{aligned} \quad (9)$$

By substituting (8) and (9) into (6), we arrive at (5), which completes the proof. \blacksquare

Remark 1: From Proposition 1, we see that under the premise of the domain transformation model (Assumption 1), null discrepancy can be attained if we can learn a model with feature satisfying separable condition on \mathcal{D}^s and \mathcal{D}^t . However, since we cannot access \mathcal{D}^t , the best we can do is to make separable condition valid over \mathcal{D}^s .

B. Overview of The Proposed RIEI Network

Guided by Proposition 1, the proposed Receiver-Independent Emitter Identification (RIEI) network is shown in Fig. 3. It consists of three main components, namely the Feature Extraction and Disentanglement (FED) module, the Emitter Classifier (EC) and the Receiver Classifier (RC).

The FED module maps the input RF waveform into a high-dimensional feature space such that the emitter-dependent feature (corresponding to Z_X) and the receiver-dependent feature (corresponding to Z_ν) are disentangled.

The EC module maps the emitter-dependent feature into an M -dimensional probability vector, which provides the confidence for predicting which emitter the input signal is from.

The RC module has a similar function as the EC module, except that the input is the receiver-dependent feature and the output is a K -dimensional vector, which provides the confidence for predicting which receiver the input signal is from. Note that after training, the RC module is discarded and only the FED and EC modules are used during the test stage.

These modules together with some judiciously designed training loss functions promote to learn a feature space Z satisfying Separable Condition in Definition 1. Specifically, three types of loss functions are considered:

- 1) The classification entropy (CE) loss, which exploits the emitters' and the receivers' label information to minimize classification error probability over \mathcal{S} .
- 2) The mutual independence (MI) loss, which promotes independence between the emitter-dependent feature and the receiver-dependent feature.
- 3) The information entropy (IE) loss, which is obtained by calculating the entropy of the EC (RC) module's output when the receiver-dependent (emitter-dependent) feature is input. By maximizing the IE loss, we hope that the EC (RC) module cannot distinguish the receivers (emitters), and thus the emitters' information is not leaked to the receiver-dependent feature, and vice versa.

We will explain these losses in detail in the sequel.

C. The Loss Functions

To proceed, let us denote by $\phi_{\theta_F}(\cdot)$, $\phi_{\theta_E}(\cdot)$ and $\phi_{\theta_R}(\cdot)$ the network function associated with the FED, the EC and RC modules, resp., and $\theta_F \in \mathbb{R}^{L_F}$, $\theta_E \in \mathbb{R}^{L_E}$ and $\theta_R \in \mathbb{R}^{L_R}$ are the corresponding network parameters. Given an input signal x , the FED output vector is denoted as

$$\phi_{\theta_F}(x) \triangleq [\phi_{\theta_F}^{(E)}(x), \phi_{\theta_F}^{(R)}(x)]. \quad (10)$$

Our goal is to learn a representation $\phi_{\theta_F}(x)$ so that the first part of $\phi_{\theta_F}(x)$, i.e. $\phi_{\theta_F}^{(E)}(x)$, corresponds to the emitter-dependent features, while the last part of $\phi_{\theta_F}(x)$, i.e. $\phi_{\theta_F}^{(R)}(x)$, corresponds to the receiver-dependent features. This is achieved through the following loss functions.

1) *Classification Entropy Loss:* The classification Entropy Loss is motivated by conditions 1) and 2) of the Separable Condition, where the feature Z_ν (resp. Z_X) should be exclusively dependent on receiver (resp. emitter), containing no information related to the emitter (resp. receiver). This specificity renders Z_ν (resp. Z_X) as effective statistics for receiver (resp. emitter) classification.

To ensure accurate classification, by passing the $\phi_{\theta_F}^{(E)}(x)$ to the emitter classifier, we have the output

$$z^E = \sigma \left(\phi_{\theta_E} \left(\phi_{\theta_F}^{(E)}(x) \right) \right) \in \mathbb{R}_+^M, \quad (11)$$

where $\sigma(\cdot)$ denotes the softmax function, i.e. $[\sigma(x)]_m = \frac{e^{x_m}}{\sum_{j=1}^M e^{x_j}}$ for $x \in \mathbb{R}^M$. Notice that z^E lies in a probabilistic simplex satisfying $[z^E]_m \geq 0$, $\sum_{m=1}^M [z^E]_m = 1$. To encourage the EC correctly classifies the emitters, the cross-entropy loss is resorted:

$$\mathcal{L}_{CE}^E = \sum_{k=1}^K \sum_{(x,y) \in \mathcal{S}^k} H(z^E, \mathbf{1}_m), \quad (12)$$

where $H(\cdot, \cdot)$ denotes the cross-entropy function $H(p, q) = -\sum_i q_i \log p_i$, and $\mathbf{1}_m \in \mathbb{R}^M$ is a one-hot vector with the m -th element being one and zeros otherwise.

Similarly, we can calculate the cross-entropy loss for classifying the receivers via the RC module as follows.

$$\mathcal{L}_{CE}^R = \sum_{k=1}^K \sum_{(x,y) \in \mathcal{S}^k} \mathbf{H}(z^R, \mathbb{1}_k), \quad (13)$$

where $z^R = \sigma\left(\phi_{\theta_R}\left(\phi_{\theta_F}^{(R)}(x)\right)\right) \in \mathbb{R}_+^K$, and the one-hot vector $\mathbb{1}_k \in \mathbb{R}^K$.

By combining (12) and (13), we get the classification entropy loss:

$$\mathcal{L}_{CE} = \mathcal{L}_{CE}^E + \mathcal{L}_{CE}^R. \quad (14)$$

2) *Information Entropy Loss*: The information entropy loss is also motivated by conditions 1) and 2) of the Separable Condition. Specifically, given an emitter, Z_X is independent of ν , containing no information about the receivers. That is, when feeding Z_X into the RC module, the RC cannot correctly identify which receiver the Z_X is from, and the classification output resembles uniform distribution. From an information theoretic point of view, the classification output attains maximum information entropy. Similarly, when feeding Z_ν into EC module, the classification output should also attain maximum information entropy. In light of this, we propose the following information entropy (IE) loss \mathcal{L}_{IE} to encourage feature disentanglement.

$$\mathcal{L}_{IE} = \mathcal{L}_{IE}^{R \rightsquigarrow E} + \mathcal{L}_{IE}^{E \rightsquigarrow R}, \quad (15)$$

where $\mathcal{L}_{IE}^{R \rightsquigarrow E}$ calculates the output entropy when the receiver-dependent feature is input into the emitter classifier, i.e.,

$$\mathcal{L}_{IE}^{R \rightsquigarrow E} = - \sum_{k=1}^K \sum_{(x,y) \in \mathcal{S}^k} z^{R \rightsquigarrow E} \odot \log(z^{R \rightsquigarrow E}), \quad (16)$$

where $z^{R \rightsquigarrow E} = \sigma\left(\phi_{\theta_E}\left(\phi_{\theta_F}^{(R)}(x)\right)\right) \in \mathbb{R}_+^M$, the $\log(\cdot)$ operation is taken on every element of its argument, and \odot denotes the element-wise product. $\mathcal{L}_{IE}^{E \rightsquigarrow R}$ calculates the output entropy when the emitter-dependent feature is input into the receiver classifier, i.e.,

$$\mathcal{L}_{IE}^{E \rightsquigarrow R} = - \sum_{k=1}^K \sum_{(x,y) \in \mathcal{S}^k} z^{E \rightsquigarrow R} \odot \log(z^{E \rightsquigarrow R}), \quad (17)$$

where $z^{E \rightsquigarrow R} = \sigma\left(\phi_{\theta_R}\left(\phi_{\theta_F}^{(E)}(x)\right)\right) \in \mathbb{R}_+^K$.

3) *Mutual Independence Loss*: The mutual independence loss is motivated by condition 3) of the Separable Condition, i.e., $Z_X \perp Z_\nu$. Proposition 1 reveals that to minimize the domain discrepancy $d_{\mathcal{H}\Delta\mathcal{H}}(\mathcal{D}^s, \mathcal{D}^t)$, it is plausible to decouple the feature space into two mutually independent subspaces, one for emitter-related feature Z_X and the other for receiver-related feature Z_ν . As such, we propose the following mutual independence loss:

$$\mathcal{L}_{MI} = \sum_{k=1}^K \sum_{(x,y) \in \mathcal{S}^k} \frac{|\langle \phi_{\theta_F}^{(E)}(x), \phi_{\theta_F}^{(R)}(x) \rangle|}{\|\phi_{\theta_F}^{(E)}(x)\| \|\phi_{\theta_F}^{(R)}(x)\|}, \quad (18)$$

where $\|\cdot\|$ denotes the Frobenius norm, and $\langle \cdot, \cdot \rangle$ denotes the inner product of two vectors.

D. Training

The overall loss function is given by

$$\mathcal{L}(\theta_F, \theta_E, \theta_R) = \mathcal{L}_{CE} + \lambda_1 \mathcal{L}_{MI} - \lambda_2 \mathcal{L}_{IE}, \quad (19)$$

where \mathcal{L}_{CE} , \mathcal{L}_{IE} and \mathcal{L}_{MI} are given in Eq. (14), (15) and (18), resp.; $\lambda_i \in \mathbb{R}_+$, $i = 1, 2$ are hyperparameters. A straightforward way to train $(\theta_F, \theta_E, \theta_R)$ is using stochastic gradient descent (SGD) to update the parameters simultaneously. However, we numerically found that SGD is not stable and usually results in poor performance for our considered loss. We guess the reason is that the feature disentanglement is much harder than conventional feature extraction task, and the former is more sensitive to the update of the classifier. Therefore, the update of the classifier and the FED should be carefully balanced. To this end, we propose an alternating training with intermediate updating scheme to optimize the network parameters. Specifically, it includes the following steps. Randomly initialize $(\theta_F^0, \theta_E^0, \theta_R^0)$ and alternately update the classifier and the feature extractor:

1) Update the classifier:

$$\theta_E^{\ell+1} \leftarrow \theta_E^\ell - \eta_E^\ell \frac{\partial \mathcal{L}_{CE}}{\partial \theta_E}, \quad (20a)$$

$$\theta_R^{\ell+1} \leftarrow \theta_R^\ell - \eta_R^\ell \frac{\partial \mathcal{L}_{CE}}{\partial \theta_R}, \quad (20b)$$

$$\theta_F^{\ell+\frac{1}{2}} \leftarrow \theta_F^\ell - \eta_F^\ell \frac{\partial \mathcal{L}_{CE}}{\partial \theta_F}, \quad (20c)$$

2) Update the feature extractor for fixed $(\theta_E^{\ell+1}, \theta_R^{\ell+1})$:

$$\theta_F^{\ell+1} \leftarrow \theta_F^{\ell+\frac{1}{2}} - \eta_F^\ell \left(\lambda_1 \frac{\partial \mathcal{L}_{MI}}{\partial \theta_F} - \lambda_2 \frac{\partial \mathcal{L}_{IE}}{\partial \theta_F} \right), \quad (21)$$

where ℓ is the iteration index and η^ℓ is the step-size for the ℓ -th iteration.

We should mention that when updating the classifier, we have also performed an intermediate update for the feature extractor in (20c). This intermediate update is crucial to stabilize the learning process, since $\theta_F^{\ell+\frac{1}{2}}$ ties up the update of the classifier and the feature extractor.

IV. DISTRIBUTED RIEI

The previous RIEI model has been developed under the premise of centralized training. In this section, we consider a more practical scenario, where all the receivers are distributed, and it is impossible for the remote receivers to transmit all the raw RF data to the server due to data privacy or bandwidth limitation. To address these challenges, in this section we leverage federated learning (FL) to train RIEI in a distributed manner.

A. Federated Learning

FL is a promising privacy-preserving distributed learning paradigm that protects privacy by learning a global model across multiple devices without exposing local datasets. In FL, each device is referred to as a client. Fig. 4 illustrates the FL framework, which includes K clients and a centralized server. The training of a global model in FL requires numerous

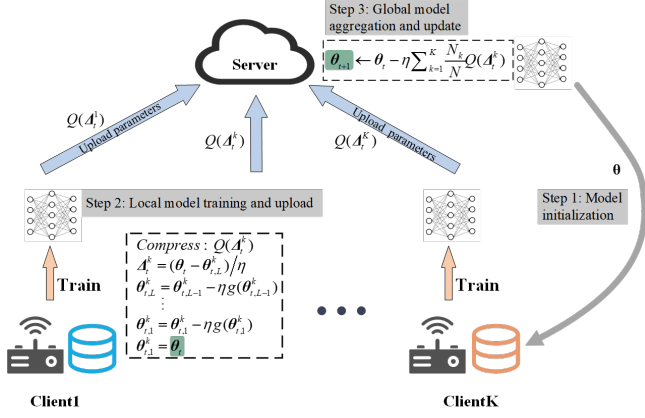


Fig. 4: The federated learning framework (with compression).

iterations involving both the server and the clients. In each iteration, the server sends an initialized global model to all clients. Each client then trains this model on its local dataset. Subsequently, the model updates from each client are sent to the centralized server and are aggregated to produce a new global model. After several iterations, the global deep learning model is well trained.

The essence of this approach lies in keeping the original RF data localized, thus safeguarding privacy and reducing the need for centralized data storage. Instead, only model updates encapsulated as gradients are exchanged between local platforms and the central server. This decentralized learning strategy not only addresses the complexity of distributed RF data, but also allows for the flexible integration of data from various sources into the training process.

B. Federated RIEI (FedRIEI)

By fitting the RIEI network into the FL framework, we can train the RIEI network in a distributed manner, and the resultant network is coined as *FedRIEI*. The detail of FedRIEI training is given in Algorithm 1, which includes two phases: server execution and client update.

Server Execution Phase. The server is used to aggregate the model gradients uploaded by the clients. To start the training, the server initializes the network parameters $\theta = \{\theta_F, \theta_E, \theta_R\}$ and distributes them to the clients. At each round, the server collects the newly-learned gradients from all clients, federated averages them to obtain the new global parameters, and broadcast them back to each client at the beginning of next round. After T rounds of server-client interaction, the parameters converge and the FedRIEI model is well-trained.

Client Update Phase. During the training process, the clients receive parameters θ from the server to train on the local data. Specifically, perform L rounds of epoch training, where L denotes the number of local training iterations at each round. The minibatch data on client k and communication round t after ℓ local updates is expressed as $S_{t,\ell}^k$. As shown in Step 4, \mathcal{L}_{CE} is used to control the training of EC, RC and FED. The parameters $\theta_E, \theta_R, \theta_F$ of EC, RC and FED are updated according to Eqn. (20). In step 5, updating the

Algorithm 1 FedRIEI Training Algorithm.

Input: RF data $\mathcal{S} = \{\mathcal{S}^k | k = 1, \dots, K\}$, one-hot vector $\mathbf{1}_m$, model parameters of the FED, EC, RC $\theta = \{\theta_F, \theta_E, \theta_R\}$, total communication rounds T , number of local steps L , clients stepsize $\eta = \{\eta_F, \eta_E, \eta_R\}$.

Output: model parameters of the FEC, EC.

Server executes:

- 1: initialize θ_0
- 2: **for** round $t = 1, 2, \dots, T$ **do**
- 3: **for** each client $k = 1, 2, \dots, K$ **in parallel do**
- 4: $\Delta_t^k \leftarrow \text{ClientUpdate}(k, \theta_t)$
- 5: **end for**
- 6: $\theta_{t+1} \leftarrow \theta_t - \eta \sum_{k=1}^K \frac{N_k}{N} Q(\Delta_t^k)$
- 7: **end for**

ClientUpdate(k, θ_t): // Run on client k

- 1: receive $\theta_t = \{\theta_F, \theta_E, \theta_R\}$ from server
- 2: **for** each local epoch $\ell = 1, 2, \dots, L$ **do**
- 3: sample one mini-batch $S_{t,\ell}^k$ from S^k
- 4: update $\theta_E, \theta_R, \theta_F$ on $S_{t,\ell}^k$ to minimize \mathcal{L}_{CE}
- 5: update θ_F on $S_{t,\ell}^k$ to minimize $\lambda_1 \mathcal{L}_{MI} - \lambda_2 \mathcal{L}_{IE}$
- 6: **end for**
- 7: compress gradient $Q(\Delta_t^k) = Q((\theta_t - \theta_{t,L}^k) / \eta_t^k)$ based on SignSGD or 1-SignSGD or ∞ -SignSGD
- 8: upload the compressed gradient to server.

parameters of FED according to Eqn. (21). After local training is completed, the model gradients for FED, EC, and RC, denoted as Δ , are compressed by the quantizer Q (cf. step 7) and the quantized gradients are uploaded to the server.

Remark 2: The compressed gradients, rather than the gradients, are sent to the server because in practice, the data link between the client and the server is usually rate-limited. After compression, the total number of transmitted bits during training can be effectively reduced. We will discuss different compression schemes, including SignSGD, 1-SignSGD and ∞ -SignSGD, and compare their performance in Section V-C2.

Remark 3: The convergence and stability of FedRIEI is guaranteed by using the convergence results in [26]. Specifically, it is shown in [26] that when ∞ -Sign and 1-Sign compression schemes are applied for client-uploaded gradients, the resultant ∞ -SignSGD and 1-SignSGD converge to stationary points (with vanishing gradients under ℓ_2 -norm measure) at rates of $\mathcal{O}(\tau^{-1/2})$ and $\mathcal{O}(\tau^{-1/3})$, resp. Here, $\tau = TL$, where T represents the number of communication rounds between the server and clients, and L denotes the number of training iterations per round performed by each client.

V. EXPERIMENTS

In this section, we conduct experiments on the publicly available Wisig dataset [17] and our own HackRF dataset to evaluate the performance of RIEI under both centralized and distributed settings.

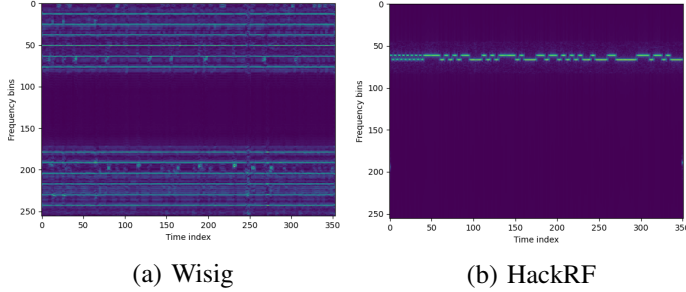


Fig. 5: The Spectrogram of signal.

A. Experimental Setup

1) **Dataset:** The Wisig dataset is constructed using WiFi nodes as emitters, emitting signals to another WiFi access point, and using multiple USRPs to receive WiFi signals. We pick a subset of the Wisig dataset with six transmitters (Tx) and six receivers (Rx). The subset is divided into six domains, each corresponding to one receiver’s data. The dataset structure is presented in Table I. As the receiver is positioned within a two-dimensional (2D) plane, the location of receivers is identified by their horizontal and vertical coordinates. For instance, the receivers situated at position (1, 1) in both horizontal and vertical planes are denoted as receiver $R_{x(1-1)}$. We perform cross-receiver tests, randomly selecting one receiver as target domain and using the other receivers as source domains. The well-trained model is tested on the target domain data.

The HackRF dataset is created by our laboratory through the open-source HackRF platform. Four HackRFs serve as emitters, and three HackRFs as receivers. The collection process involves Matlab, with signals generated at a 2.5GHz frequency. Signals are modulated using BFSK at a 2MHz sampling rate. Amplitude and frequency noise are added uniformly to introduce randomness. Data is randomly partitioned for training and testing, similar to the Wisig dataset. The signal spectrum of the Wisig dataset and HackRF dataset are shown in Fig. 5. Table I provides an overview of the HackRF dataset structure.

TABLE I: The overall structure of the Wisig and HackRF dataset.

Parameter	Wisig	HackRF
Emitter	6	4
Receiver	6	3
Input sample dimension	2×256	$2 \times 224 \times 224$
Training samples per receiver	14400	3200
Testing samples per receiver	4800	800

2) **Model setup:** The FED employs Residual Networks (ResNets) [27] for both the Wisig and HackRF datasets. Both one-dimensional temporal data and two-dimensional time-frequency spectrogram data are considered as input. Specifically, ResNet1D-18 and ResNet50 with attention are utilized as FED modules when the input data is in the two-dimensional time-frequency spectrogram form. When the input data is in the one-dimensional temporal form, we replace the 2D-

convolution with 1D-convolution in ResNet to better accommodate the one-dimensional time series of RF signals. Both the EC and RC networks are implemented with three-layer fully connected networks. The hyperparameters including the initial learning rate η of the FED, EC, RC are all 0.0001. Additionally, both λ_1 and λ_2 in Eq. (19) are set to 1.2 to optimize the model performance.

B. Performance of Centralized Scenario

1) **Comparison with Existing Methods:** We first carry out the classification experiments on the centralized network to demonstrate the benefits of RIEI by comparing it with the baseline method [15], the receiver-agnostic RFFI method based on Domain-Adversarial Neural Networks (DANN) [16], and the statistical distancebased receiver-agnostic (SD-RXA) method [28]. The baseline method treats all the multi-source data as a whole, and trains an RFFI model by minimizing the cross-entropy loss. The DANN method aims at learning the feature representation while reducing the distributional differences between the source and target domains through adversarial training. The SD-RXA optimizes the feature extractor to ensure that the extracted receiver-related and emitter-related features tend to come from distributions with significant statistical distances. In the Wisig and HackRF experiments, we feed the models with time-domain signals and time-frequency diagrams obtained through Short-time Fourier Transform (STFT). The experimental design entails training the model on data from two receivers, followed by testing on data from a third receiver. To evaluate the model, we take into account the mean and standard deviation of the classification accuracy for the last 5 epochs.

In Table II, we present the computational complexity, model parameter counts, and the classification accuracy of RIEI, SD-RXA, DANN, and the baseline method on the HackRF dataset. The data in the HackRF i column were tested using data from the HackRF i receiver and trained using data from the remaining two receivers. For computational complexity, we use FLOPs (floating point operations per second) as the metric. It can be seen that the difference in computational complexity between RIEI, SD-RXA, DANN, and the baseline method is not significant. As for the recognition accuracy, the results clearly show that RIEI outperforms the other three methods. Particularly, when the inputs are time-domain signals, RIEI achieves an average improvement of 10.84% over the baseline, 6.77% over DANN, and 3.56% over SD-RXA. When the inputs are time-frequency diagrams, it improves by an average of 20.74% compared to the baseline, 2.15% compared to DANN, and 2.24% compared to SD-RXA.

Table III and Table IV show the classification accuracy for the tasks on the Wisig dataset. Again, RIEI outperforms the other three methods. Particularly, when using time-domain signals as inputs, RIEI achieves an average improvement of 9.37%, 8.38% and 5.83% over the baseline, DANN and SD-RXA methods, resp. With time-frequency diagrams as inputs, it improves by an average of 9.49%, 6.28% and 4.27% compared to the baseline, DANN and SD-RXA, resp.

Based on the above results, it can be seen that the overall recognition performance is better when one-dimensional tem-

TABLE II: Comparison of Performance on the HackRF dataset.

Input Data Form	Feature Extraction	Model	FLOPs(M)	Params(M)	HackRF 1 Acc(%)	HackRF 2 Acc(%)	HackRF 3 Acc(%)
One-dim. temporal signal	ResNet1D-18	Baseline	0.799	0.022	57.73 ± 3.37	68.40 ± 3.65	49.98 ± 0.12
		DANN	0.866	0.088	61.92 ± 5.11	74.08 ± 3.37	52.30 ± 2.54
		SD-RXA	0.933	0.156	63.38 ± 0.78	72.00 ± 0.75	62.55 ± 0.32
		RIEI	0.867	0.089	69.92 ± 4.55	74.48 ± 5.48	64.22 ± 4.76
Two-dim. time-frequency diagram	ResNet50	Baseline	4095	26.13	34.56 ± 2.44	54.81 ± 2.44	54.24 ± 6.76
		DANN	4095	26.19	55.15 ± 1.46	75.68 ± 3.85	68.55 ± 0.65
		SD-RXA	4095	26.26	52.73 ± 0.73	76.03 ± 0.86	70.35 ± 0.46
		RIEI	4095	26.20	53.41 ± 5.21	79.21 ± 6.79	73.22 ± 2.60

poral signals are used as input. This may be due to electromagnetic signals are temporal sequences, and one-dimensional feature extraction networks can effectively capture local characteristics and temporal dependencies within the time series.

2) *Ablation Studies*: Ablation studies are conducted to demonstrate the efficacy of various components in RIEI. As presented in Table V, the notation $(H_i, H_j) \rightarrow H_k$ indicates that the model is trained using data from HackRF receivers i and j , and tested with data from HackRF receiver k , while $(Rx_{(x-y)}, Rx_{(x'-y')}) \rightarrow Rx_{(x''-y'')}$ signifies an identical process. Results indicate that using either information entropy loss or mutual independence loss alone results in an improved recognition accuracy of 14.79% and 14.09%, resp. Combining both loss functions results in recognition accuracy improvement of 18.16% compared to the baseline model. Furthermore, using both loss functions has better results compared to using only one of them, with accuracy improved by 3.38% and 4.08%, resp. It is therefore concluded that both information entropy loss and mutual independence loss are effective for optimizing network performance.

3) *t-SNE Visualization*: In this example, we show case that the proposed RIEI model indeed disentangles the features of emitters and receivers by drawing the scatter plot of the dimension-reduced emitter-dependent features. For illustration, we use HackRF 1 and HackRF 2 to train the model and test it on HackRF 3. Fig. 6(a)-Fig. 6(c) show the emitter-dependent features obtained by t-distributed Stochastic Neighbor Embedding (t-SNE) with different colors representing different emitters. As seen, the emitter-dependent features of HackRF 3 follow a similar distribution as HackRF 1 and HackRF 2, which implies that the proposed model can effectively mitigate the effect of receivers and make the feature distributed consistently over different receivers. By contrast, Fig. 6(d) presents the t-SNE visualization obtained by the baseline method. Clearly, different emitters' features are densely overlapped due to the ignorance of the receiver effect.

4) *Robustness Test*: In a wireless communication environment, the signal may be subject to various kinds of interference. In order to verify the robustness of the model, we consider adding two types of disturbances to the original signal: narrowband hopping interference and broadband Gaussian noise. Narrowband hopping interference randomly and uniformly selects part of the frequency band to interfere. In our simulation, the whole signal frequency band is divided into 256 frequency bins and 2 of them are selected. The selection

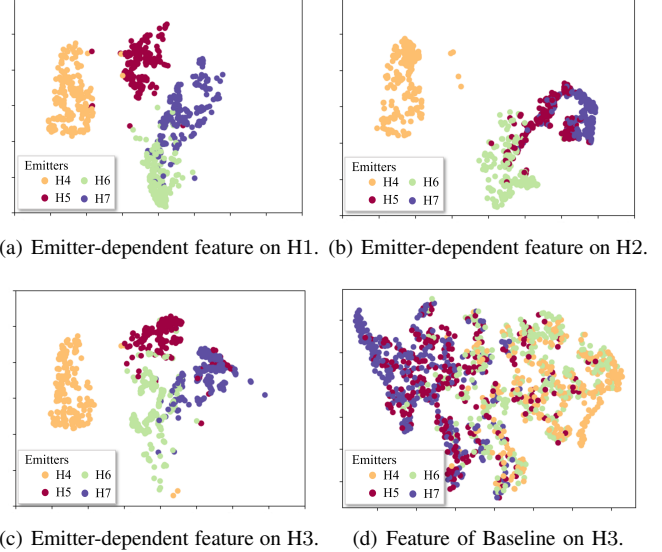


Fig. 6: Visualization with t-SNE of emitter-dependent features. Different colors represent the features of different emitters.

is consistent within each data sample but varies randomly between samples. Broadband Gaussian noise adds Gaussian noise across the entire frequency band of the signal.

Fig. 7 shows the recognition performance of RIEI under different interference-to-signal power ratios (ISRs). From the figure, we see that the recognition accuracy of RIEI decreases as the ISR increases. Nevertheless, for a wide range of the ISR the recognition performance is quite stable, which implies that the proposed model RIEI model is not very sensitive to the disturbances. Moreover, it can also be observed that the narrowband interference has less impact on recognition performance compared to the broadband noise. This may be due to the narrowband interference only affects a small portion of the signal spectrum, leaving most of the frequency components intact, thereby causing relatively less disruption to the overall features and information of the signal.

C. Performance of Distributed Scenario

1) *Comparison with Baseline*: We apply the baseline method mentioned in the previous subsection to the distributed scenario as the federated baseline network, referred to as FedBase. In the distributed setting, we compare FedRIEI with the centralized RIEI and FedBase. For simplicity, in

TABLE III: Comparison of recognition accuracy (%) on the Wisig dataset (Time-domain signal).

Training receivers	Test receiver	Baseline	DANN	SD-RXA	RIEI
$Rx_{(1-1)}, Rx_{(7-7)}$	$Rx_{(1-19)}$	70.39 ± 1.37	72.15 ± 0.36	73.70 ± 0.33	77.88 ± 2.23
$Rx_{(1-1)}, Rx_{(8-8)}$	$Rx_{(1-19)}$	62.85 ± 0.75	62.52 ± 0.32	70.53 ± 0.88	79.43 ± 1.66
$Rx_{(1-1)}, Rx_{(14-7)}$	$Rx_{(1-19)}$	64.78 ± 0.72	63.43 ± 0.11	64.63 ± 0.35	66.09 ± 0.67
$Rx_{(7-7)}, Rx_{(8-8)}$	$Rx_{(1-19)}$	69.16 ± 1.26	71.72 ± 1.18	68.04 ± 1.20	70.51 ± 3.53
$Rx_{(7-7)}, Rx_{(14-7)}$	$Rx_{(1-19)}$	65.34 ± 0.54	64.89 ± 0.19	68.10 ± 0.68	77.35 ± 1.53
$Rx_{(8-8)}, Rx_{(14-7)}$	$Rx_{(1-19)}$	62.51 ± 0.80	63.67 ± 0.34	65.16 ± 0.13	75.48 ± 1.21
$Rx_{(1-1)}, Rx_{(1-19)}$	$Rx_{(14-7)}$	66.54 ± 1.31	70.75 ± 0.61	71.69 ± 0.25	71.91 ± 2.08
$Rx_{(1-1)}, Rx_{(7-7)}$	$Rx_{(14-7)}$	60.49 ± 1.57	58.18 ± 0.86	66.40 ± 0.49	68.33 ± 2.37
$Rx_{(1-1)}, Rx_{(8-8)}$	$Rx_{(14-7)}$	61.10 ± 0.56	63.18 ± 0.46	64.84 ± 0.26	73.54 ± 1.27
$Rx_{(1-19)}, Rx_{(7-7)}$	$Rx_{(14-7)}$	62.97 ± 1.89	61.65 ± 0.55	63.20 ± 0.31	73.52 ± 3.15
$Rx_{(1-19)}, Rx_{(8-8)}$	$Rx_{(14-7)}$	65.61 ± 2.41	66.51 ± 0.20	68.40 ± 0.19	72.05 ± 2.71
$Rx_{(7-7)}, Rx_{(8-8)}$	$Rx_{(14-7)}$	55.31 ± 1.48	60.23 ± 0.25	64.85 ± 1.07	73.46 ± 2.00

TABLE IV: Comparison of recognition accuracy (%) on the Wisig dataset (Time-frequency diagram).

Training receivers	Test receiver	Baseline	DANN	SD-RXA	RIEI
$Rx_{(1-1)}, Rx_{(7-7)}$	$Rx_{(1-19)}$	68.56 ± 0.55	68.71 ± 0.53	69.44 ± 0.34	70.71 ± 0.89
$Rx_{(1-1)}, Rx_{(8-8)}$	$Rx_{(1-19)}$	56.69 ± 0.30	66.71 ± 0.83	67.34 ± 0.66	73.70 ± 0.92
$Rx_{(1-1)}, Rx_{(14-7)}$	$Rx_{(1-19)}$	55.68 ± 0.80	59.49 ± 0.81	64.00 ± 1.09	64.92 ± 0.41
$Rx_{(7-7)}, Rx_{(8-8)}$	$Rx_{(1-19)}$	62.16 ± 0.53	68.08 ± 0.50	67.67 ± 1.24	64.75 ± 0.88
$Rx_{(7-7)}, Rx_{(14-7)}$	$Rx_{(1-19)}$	66.90 ± 1.05	67.23 ± 0.83	67.17 ± 0.47	74.70 ± 1.65
$Rx_{(8-8)}, Rx_{(14-7)}$	$Rx_{(1-19)}$	63.87 ± 0.31	63.99 ± 0.29	63.56 ± 0.46	68.31 ± 0.57
$Rx_{(1-1)}, Rx_{(1-19)}$	$Rx_{(14-7)}$	57.77 ± 1.21	58.73 ± 0.89	60.90 ± 0.86	77.69 ± 1.69
$Rx_{(1-1)}, Rx_{(7-7)}$	$Rx_{(14-7)}$	58.61 ± 0.21	65.31 ± 0.96	70.08 ± 0.85	73.79 ± 1.10
$Rx_{(1-1)}, Rx_{(8-8)}$	$Rx_{(14-7)}$	44.42 ± 1.15	49.11 ± 0.76	53.87 ± 0.80	52.71 ± 0.64
$Rx_{(1-19)}, Rx_{(7-7)}$	$Rx_{(14-7)}$	45.25 ± 0.76	49.94 ± 1.39	45.19 ± 0.87	52.05 ± 0.89
$Rx_{(1-19)}, Rx_{(8-8)}$	$Rx_{(14-7)}$	52.26 ± 0.32	51.40 ± 0.50	58.76 ± 1.40	60.11 ± 1.04
$Rx_{(7-7)}, Rx_{(8-8)}$	$Rx_{(14-7)}$	56.68 ± 0.72	58.58 ± 0.90	61.32 ± 1.15	67.10 ± 1.32

TABLE V: Comparison of recognition accuracy (%) of ablation studies.

Components		(H1, H2)	(H1, H3)	(H2, H3)	$(Rx_{(1-1)}, Rx_{(8-8)})$	$(Rx_{(7-7)}, Rx_{(14-7)})$	$(Rx_{(7-7)}, Rx_{(8-8)})$
IE	MI	→ H3	→ H2	→ H1	→ $Rx_{(1-19)}$	→ $Rx_{(1-19)}$	→ $Rx_{(14-7)}$
×	×	54.24 ± 6.76	54.81 ± 2.44	34.56 ± 2.44	62.85 ± 0.75	65.34 ± 0.54	55.31 ± 1.48
✓	×	67.30 ± 14.17	72.14 ± 10.14	52.77 ± 6.98	76.94 ± 0.86	74.53 ± 0.76	72.15 ± 1.23
×	✓	72.40 ± 4.10	72.90 ± 4.90	52.25 ± 4.63	77.74 ± 1.41	68.12 ± 2.32	68.21 ± 1.56
✓	✓	73.22 ± 2.60	79.21 ± 6.79	53.41 ± 5.21	79.43 ± 1.66	77.35 ± 1.53	73.46 ± 2.00

TABLE VI: Comparison of recognition accuracy (%) for four receivers training and another receiver testing.

Training data receivers	Test data receiver	FedBase accuracy	Centralized RIEI accuracy	FedRIEI accuracy
$Rx_{(1-1)}, Rx_{(1-19)}, Rx_{(7-7)}, Rx_{(8-8)}$	$Rx_{(14-7)}$	62.11 ± 0.09	73.31 ± 2.22	76.54 ± 0.26
$Rx_{(1-1)}, Rx_{(1-19)}, Rx_{(7-7)}, Rx_{(14-7)}$	$Rx_{(8-8)}$	66.35 ± 0.46	67.76 ± 3.63	69.83 ± 0.88
$Rx_{(1-1)}, Rx_{(1-19)}, Rx_{(8-8)}, Rx_{(14-7)}$	$Rx_{(7-7)}$	62.39 ± 0.65	79.04 ± 1.36	75.07 ± 0.85
$Rx_{(1-1)}, Rx_{(7-7)}, Rx_{(8-8)}, Rx_{(14-7)}$	$Rx_{(1-19)}$	60.18 ± 0.95	68.21 ± 1.02	75.32 ± 1.26
$Rx_{(1-19)}, Rx_{(7-7)}, Rx_{(8-8)}, Rx_{(14-7)}$	$Rx_{(1-1)}$	64.87 ± 1.03	76.29 ± 0.34	75.32 ± 0.55

this subsection all the federated models are trained without gradient compression, and the performance comparison with compression will be discussed in the next subsection.

Assuming there are four clients in training phase, each using the dataset of one receiver. At each iteration, each client first downloads the global model from the server; then it trains locally once to obtain the local gradient; at last, each client uploads its local gradient to the central server, where a new global model is obtained. The above process repeats until some convergence criterion is met. In test phase, the well-trained model is tested on the dataset from the fifth receiver. Therefore, for FedRIEI, it differs from the RIEI model only in the training stage, where some additional message exchange and parameter aggregation are needed. However, for the inference stage,

FedRIEI and RIEI have the same complexity.

In Table VI, we present the classification accuracy achieved by FedBase, RIEI, and FedRIEI approaches. The results clearly depict a penchant for FedRIEI to outperform the FedBase in terms of recognition accuracy, with an average improvement of 11.24%. Compared to centralized RIEI, FedRIEI demonstrates superior performance. This is probably attributed to the utilization of Batch Normalization (BN) layers, which play the role of preventing gradient vanishing/exploding and accelerating network training. For centralized RIEI, the BN utilizes all the data in a minibatch of size 64 to calculate a single scaling factor for different receivers' data within the minibatch. By contrast, the BN of FedRIEI is conducted locally at each client with a smaller minibatch size of 16, and

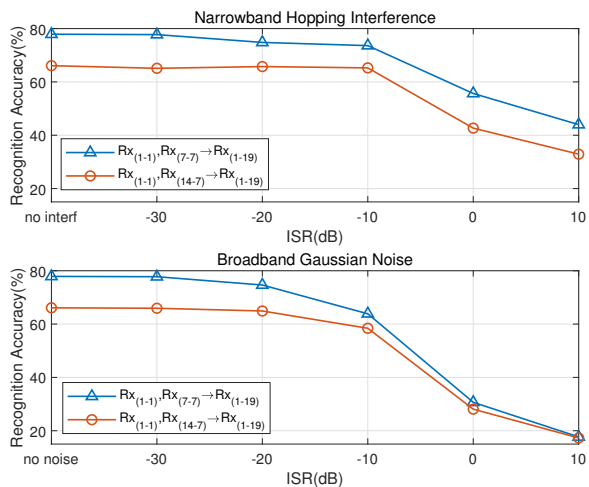


Fig. 7: The recognition accuracy of RIEI under different ISR.

different normalization factors are utilized by clients. Therefore, the BN of FedRIEI has more degrees of freedom and more fine-controlled minibatch size than that of centralized RIEI, which help train a better generalizable RFFI model on the unseen target domain.

2) *Comparison with Gradient Compression*: In this subsection, we investigate the impact of gradient compression on the performance of FedRIEI. We focus on one-bit quantization and compare several one-bit compression schemes, including SignSGD [29], 1–SignSGD [26] and ∞ –SignSGD [26]. SignSGD is a scheme that directly takes the sign of each coordinate of the gradient. For any $x \in \mathbb{R}$, the sign operator is defined as: $Sign(x) = 1$ if $x \geq 0$ and -1 otherwise; 1–SignSGD intentionally adds Gaussian noise $\xi \sim \mathcal{CN}(0, \sigma^2)$ to the gradient before performing sign quantization, i.e. $Sign(x + \xi)$; ∞ –SignSGD is similar to 1–SignSGD, except that the noise follows uniform distribution.

Table VII presents the performance of various gradient compression methods. It can be observed that the performance loss is minimal when compressing the gradients before uploading them to the server, with more pronounced losses only apparent when generalizing to the receiver $Rx_{(1-19)}$. Additionally, the approach of first adding noise to local gradients before applying the sign operation outperforms the direct signing of individual elements in the gradient. For the generalization to the receiver $Rx_{(1-19)}$, we adjusted the noise variance of 1–SignSGD and ∞ –SignSGD. Fig. 8 shows the performance of 1–SignSGD and ∞ –SignSGD when generalizing to the receiver $Rx_{(1-19)}$ with different noise variances. It can be seen that as the noise variance increases, the classification accuracy increases and then decreases, reaching a maximum close to the performance without gradient compression, both outperforming signSGD. Fig. 9 plots the testing accuracy of all methods versus the accumulated number of bits transmitted from the clients to the server. One can see that the three gradient compression methods significantly enhance communication efficiency, with minimal performance loss for uncompressed FedRIEI.

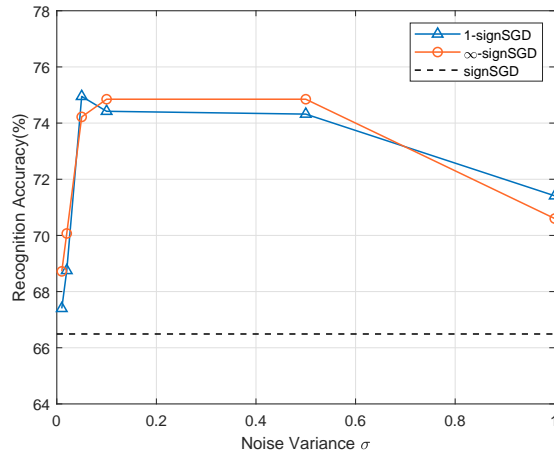
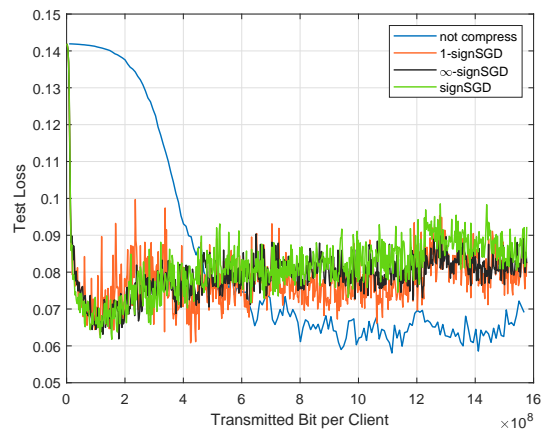
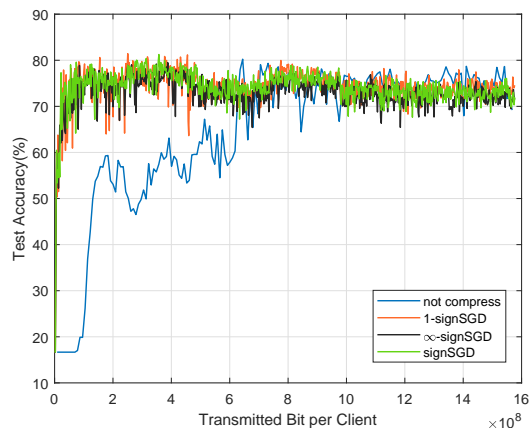


Fig. 8: The recognition accuracy of different gradient compression methods when generalizing to the receiver $Rx_{(1-19)}$ with different noise variances.



(a) Test Loss v.s. bits



(b) Test Accuracy v.s. bits

Fig. 9: Performance of FedRIEI with different gradient compression methods when generalizing ($Rx_{(1-1)}$, $Rx_{(1-19)}$, $Rx_{(7-7)}$, $Rx_{(8-8)}$) to $Rx_{(14-7)}$.

TABLE VII: Comparison of recognition accuracy (%) for different gradient compression methods.

Training data receivers	Test data receiver	FedRIEI	SignSGD	1-SignSGD $\sigma = 0.01$	∞ -SignSGD $\sigma = 0.01$
$Rx_{(1-1)}$, $Rx_{(1-19)}$, $Rx_{(7-7)}$, $Rx_{(8-8)}$	$Rx_{(14-7)}$	76.54 ± 0.26	75.71 ± 1.04	76.90 ± 0.97	74.80 ± 0.74
$Rx_{(1-1)}$, $Rx_{(1-19)}$, $Rx_{(7-7)}$, $Rx_{(14-7)}$	$Rx_{(8-8)}$	69.83 ± 0.88	66.99 ± 0.80	67.63 ± 0.43	67.11 ± 0.31
$Rx_{(1-1)}$, $Rx_{(1-19)}$, $Rx_{(8-8)}$, $Rx_{(14-7)}$	$Rx_{(7-7)}$	75.07 ± 0.85	70.10 ± 1.69	73.90 ± 1.45	73.35 ± 0.67
$Rx_{(1-1)}$, $Rx_{(7-7)}$, $Rx_{(8-8)}$, $Rx_{(14-7)}$	$Rx_{(1-19)}$	75.32 ± 1.26	66.49 ± 0.60	67.40 ± 0.88	68.72 ± 0.95
$Rx_{(1-19)}$, $Rx_{(7-7)}$, $Rx_{(8-8)}$, $Rx_{(14-7)}$	$Rx_{(1-1)}$	75.32 ± 0.55	75.36 ± 0.77	75.26 ± 0.68	75.55 ± 0.58

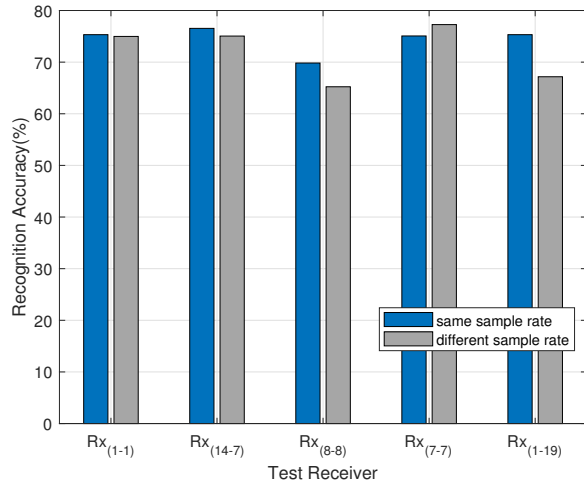


Fig. 10: The recognition accuracy of FedRIEI when four receivers are used for training and one for testing. “Same sampling rate” refers to all receivers operating at the same sampling rate, while “different sampling rates” indicates that each receiver operates at different sampling rate.

3) *Effect of Sampling Rate*: In practice, each receiver/client may record signals at different rates. To investigate the impact of different sampling rates on FedRIEI performance, we set $Rx_{(1-1)}$ as the original sampling rate, while $Rx_{(1-19)}$ operated at 0.6 times, $Rx_{(7-7)}$ at 0.7 times, $Rx_{(8-8)}$ at 0.8 times, and $Rx_{(14-7)}$ at 0.9 times the original rate. To keep all the receivers having the same signal length, cubic spline interpolation is first performed at all the receivers except $Rx_{(1-1)}$. Fig. 10 shows the recognition accuracy when four receivers are used for training and the remaining one for testing. For comparison, the recognition accuracy corresponding to the same sampling rate at all the receivers is also plotted. It can be seen that varied sampling rates at the receivers have little impact on FedRIEI’s recognition accuracy.

VI. CONCLUSIONS AND DISCUSSIONS

This paper has addressed the fingerprint contamination problem, which arises from different characteristics of receivers in Radio Frequency Fingerprint Identification (RFFI). Based on a theoretical analysis of the cross-receiver RFFI problem, we designed an RIEI model to achieve cross-receiver RFFI. The main idea of RIEI is to separate the receiver-related features from the emitter-related features by feature disentanglement. To this end, we have developed three specially designed losses, namely the cross-entropy loss, the

mutual independence loss and the information entropy loss, to encourage the model to learn a receiver-independent feature space and thus address the challenge of generalizing to unseen receivers during the deployment phase. Moreover, considering practical limitation on centralized processing, we also extend RIEI to a distributed scenario to eliminate the need for centralized servers to access local raw data. Simulation results on real-world datasets demonstrated the effectiveness of RIEI and FedRIEI in suppressing the effect of receiver on RFFI.

However, we should also note that for excessively high ISR (cf. Fig. 7), the recognition performance drops significantly. Therefore, as a future work, it is worth investigating how to further robustify the RIEI model under extremely interfered scenarios.

VII. ACKNOWLEDGMENT

The authors would like to sincerely thank the anonymous reviewers for their helpful and insightful comments.

REFERENCES

- [1] H. Liu, S. Zhu, L. Yang, Q. Li, and J. Lin, “Receiver-agnostic radio frequency fingerprint identification via feature disentanglement,” in *2023 IEEE 24th International Workshop on Signal Processing Advances in Wireless Communications (SPAWC)*. IEEE, 2023, pp. 46–50.
- [2] S. Sicari, A. Rizzardi, L. A. Grieco, and A. Coen-Porisini, “Security, privacy and trust in internet of things: The road ahead,” *Computer networks*, vol. 76, pp. 146–164, 2015.
- [3] M. B. Yassein, S. Aljawarneh, E. Qawasmeh, W. Mardini, and Y. Khamaysch, “Comprehensive study of symmetric key and asymmetric key encryption algorithms,” in *2017 international conference on engineering and technology (ICET)*. IEEE, 2017, pp. 1–7.
- [4] S. Li, L. D. Xu, and S. Zhao, “The internet of things: a survey,” *Information systems frontiers*, vol. 17, pp. 243–259, 2015.
- [5] L. Peng, A. Hu, J. Zhang, Y. Jiang, J. Yu, and Y. Yan, “Design of a hybrid rf fingerprint extraction and device classification scheme,” *IEEE internet of things journal*, vol. 6, no. 1, pp. 349–360, 2018.
- [6] A. C. Polak and D. L. Goeckel, “Identification of wireless devices of users who actively fake their rf fingerprints with artificial data distortion,” *IEEE Transactions on Wireless Communications*, vol. 14, no. 11, pp. 5889–5899, 2015.
- [7] Y. Zou, J. Zhu, X. Wang, and L. Hanzo, “A survey on wireless security: Technical challenges, recent advances, and future trends,” *Proceedings of the IEEE*, vol. 104, no. 9, pp. 1727–1765, 2016.
- [8] N. Soltanieh, Y. Norouzi, Y. Yang, and N. C. Karmakar, “A review of radio frequency fingerprinting techniques,” *IEEE Journal of Radio Frequency Identification*, vol. 4, no. 3, pp. 222–233, 2020.
- [9] K. Ellis and N. Serinken, “Characteristics of radio transmitter fingerprints,” *Radio Science*, vol. 36, no. 4, pp. 585–597, 2001.
- [10] J. Hall, M. Barbeau, E. Kranakis *et al.*, “Detection of transient in radio frequency fingerprinting using signal phase,” *Wireless and optical communications*, vol. 9, p. 13, 2003.
- [11] S. Dolatshahi, A. Polak, and D. L. Goeckel, “Identification of wireless users via power amplifier imperfections,” in *2010 Conference Record of the Forty Fourth Asilomar Conference on Signals, Systems and Computers*. IEEE, 2010, pp. 1553–1557.

- [12] I. O. Kennedy, P. Scanlon, F. J. Mullany, M. M. Buddhikot, K. E. Nolan, and T. W. Rondeau, "Radio transmitter fingerprinting: A steady state frequency domain approach," in *2008 IEEE 68th Vehicular Technology Conference*. IEEE, 2008, pp. 1–5.
- [13] G. Shen, J. Zhang, A. Marshall, and J. R. Cavallaro, "Towards scalable and channel-robust radio frequency fingerprint identification for lora," *IEEE Transactions on Information Forensics and Security*, vol. 17, pp. 774–787, 2022.
- [14] L. Peng, J. Zhang, M. Liu, and A. Hu, "Deep learning based rf fingerprint identification using differential constellation trace figure," *IEEE Transactions on Vehicular Technology*, vol. 69, no. 1, pp. 1091–1095, 2019.
- [15] A. Al-Shawabka, F. Restuccia, S. D'Oro, T. Jian, B. C. Rendon, N. Soltani, J. Dy, S. Ioannidis, K. Chowdhury, and T. Melodia, "Ex-posing the fingerprint: Dissecting the impact of the wireless channel on radio fingerprinting," in *IEEE INFOCOM 2020-IEEE Conference on Computer Communications*. IEEE, 2020, pp. 646–655.
- [16] G. Shen, J. Zhang, A. Marshall, R. Woods, J. Cavallaro, and L. Chen, "Towards receiver-agnostic and collaborative radio frequency fingerprint identification," *IEEE Transactions on Mobile Computing*, 2023.
- [17] S. Hanna, S. Karunaratne, and D. Cabric, "Wisig: A large-scale wifi signal dataset for receiver and channel agnostic rf fingerprinting," *IEEE Access*, vol. 10, pp. 22 808–22 818, 2022.
- [18] X. Zha, T. Li, Z. Qiu, and F. Li, "Cross-receiver radio frequency fingerprint identification based on contrastive learning and subdomain adaptation," *IEEE Signal Processing Letters*, vol. 30, pp. 70–74, 2023.
- [19] L. Yang, Q. Li, X. Ren, Y. Fang, and S. Wang, "Mitigating receiver impact on radio frequency fingerprint identification via domain adaptation," *IEEE Internet of Things Journal*, vol. 11, no. 13, pp. 24 024–24 034, 2024.
- [20] J. Bao, X. Xie, Z. Lu, J. Hong, and C. Hua, "Receiver-agnostic radio frequency fingerprinting based on two-stage unsupervised domain adaptation and fine-tuning," in *GLOBECOM 2023-2023 IEEE Global Communications Conference*. IEEE, 2023, pp. 6085–6090.
- [21] G. Shen, J. Zhang, A. Marshall, R. Woods, J. Cavallaro, and L. Chen, "Towards receiver-agnostic and collaborative radio frequency fingerprint identification," *IEEE Transactions on Mobile Computing*, 2023.
- [22] K. Merchant and B. Noursain, "Toward receiver-agnostic rf fingerprint verification," in *2019 IEEE Globecom Workshops (GC Wkshps)*. IEEE, 2019, pp. 1–6.
- [23] J. Wang, C. Lan, C. Liu, Y. Ouyang, T. Qin, W. Lu, Y. Chen, W. Zeng, and P. Yu, "Generalizing to unseen domains: A survey on domain generalization," *IEEE Transactions on Knowledge and Data Engineering*, 2022.
- [24] B. McMahan, E. Moore, D. Ramage, S. Hampson, and B. A. y Arcas, "Communication-efficient learning of deep networks from decentralized data," in *Artificial intelligence and statistics*. PMLR, 2017, pp. 1273–1282.
- [25] A. Robey, G. J. Pappas, and H. Hassani, "Model-based domain generalization," *Advances in Neural Information Processing Systems*, vol. 34, pp. 20 210–20 229, 2021.
- [26] Z. Tang, Y. Wang, and T.-H. Chang, "z-signfedavg: A unified stochastic sign-based compression for federated learning," *arXiv preprint arXiv:2302.02589*, 2023.
- [27] K. He, X. Zhang, S. Ren, and J. Sun, "Deep residual learning for image recognition," in *Proceedings of the IEEE conference on computer vision and pattern recognition*, 2016, pp. 770–778.
- [28] T. Zhao, S. Sarkar, E. Krijestorac, and D. Cabric, "GAN-RXA: A practical scalable solution to receiver-agnostic transmitter fingerprinting," *IEEE Transactions on Cognitive Communications and Networking*, vol. 10, no. 2, pp. 403–416, 2024.
- [29] J. Bernstein, Y.-X. Wang, K. Azizzadenesheli, and A. Anandkumar, "signsgd: Compressed optimisation for non-convex problems," in *International Conference on Machine Learning*. PMLR, 2018, pp. 560–569.



Ying Zhang received the B.Eng. degree from Chongqing University of Posts and Telecommunications, Chongqing, China, in 2014, and the M.S. degree in electronic and communication engineering from the University of Electronic Science and Technology of China (UESTC), Chengdu, China, in 2017. She is currently pursuing the Ph.D. degree at the School of Information and Communication Engineering, UESTC. Her research interests include wireless communications and signal processing.



Qiang Li received the B.Eng. and M.Phil. degrees in communication and information engineering from the University of Electronic Science and Technology of China (UESTC), Chengdu, China, and the Ph.D. degree in electronic engineering from the Chinese University of Hong Kong (CUHK), Hong Kong, in 2005, 2008, and 2012, respectively. He was a Visiting Scholar with the University of Minnesota, and a Research Associate with the Department of Electronic Engineering and the Department of Systems Engineering and Engineering Management, CUHK. Since November 2013, he has been with the School of Information and Communication Engineering, UESTC, where he is currently a Professor. His recent research interests focus on machine learning and intelligent signal processing in wireless communications. He received the First Prize Paper Award in the IEEE Signal Processing Society Postgraduate Forum Hong Kong Chapter in 2010, a Best Paper Award of IEEE PIMRC in 2016, and the Best Paper Award of the IEEE SIGNAL PROCESSING LETTERS in 2016.



Hongli Liu received the B.Eng. degree from the Southwest University, Chongqing, China, in 2022. She is currently working toward the Ph.D. degree at the School of Information and Communication Engineering, University of Electronic Science and Technology of China, Chengdu, China. Her research interests are mainly on wireless communications, massive MIMO systems, and integrated sensing and communication.



Liu Yang received the B.Eng. degree from the University of Electronic Science and Technology of China (UESTC), Chengdu, China, in 2020. He is currently pursuing the Ph.D. degree with the School of Information and Communication Engineering, UESTC. His current research interests include signal processing and radio frequency fingerprint identification.



Jian Yang received the B.S. and M.S. degrees in communication and information systems from Information Engineering University, Zhengzhou, China, in 2003 and 2006, respectively. After his graduation, he joined the Northern Institute of Electronic Equipment of China, Beijing, China. He is currently pursuing the Ph.D. degree with the School of Cyberspace Science and Technology, Beijing Institute of Technology, Beijing, China. He is mainly interested in communication signal processing.